# Heterogeneous Interaction and Reaction of HOBr on Ice Films

**Liang Chu and Liang T. Chu***

*Department of Environmental Health and Toxicology, State University of New York at Albany and Wadsworth Center, P.O. Box 509, Albany, New York 12201-0509*

*Received: April 2, 1999; In Final Form: July 28, 1999*

The uptake coefficient $\gamma$ of HOBr on the ice surface from 190 to 239 K has been investigated in a flow reactor interfaced with a differentially pumped quadrupole mass spectrometer. $\gamma$ of HOBr on ice is in the range $0.11-7 \times 10^{-3}$ at 190−218 K and is in the range $2 \times 10^{-3}$ to $6 \times 10^{-4}$ at 223−239 K. The desorption temperature $T_d$ of HOBr on the ice film was determined. $T_d$ increases with the HOBr exposure. The Monte Carlo simulation was used to shed light on the nature of the desorption and gas−surface interactions. This study extends our investigations to the reaction probability of the HOBr + HCl reaction. The reaction probability ranges from 0.05 to 0.23 at 190 K and 0.004 to 0.19 at 222 K as a function of $P_{HCl}$, which varies from $1.3 \times 10^{-7}$ to $8.8 \times 10^{-6}$ Torr and $4.2 \times 10^{-7}$ to $1.5 \times 10^{-5}$ Torr, respectively. Kinetic analysis indicates that the heterogeneous reaction of HOBr + HCl follows the Langmuir−Hinshelwood type.

## I. Introduction

The heterogeneous conversion of photochemically inactive and chlorine bromine reservoir compounds into photochemically active forms is related to the occurrence of the Antarctic ozone hole.[1,2] Over the past decade, the heterogeneous chemistry of chlorine has been studied extensively.[2−7] Heterogeneous reaction of $ClONO_2 + HCl(s) \rightarrow Cl_2 + HNO_3(s)$ on polar stratospheric cloud (PSC) surfaces was originally proposed to be important in converting inactive chlorine to an active form which subsequently depletes polar ozone through catalytic cycles.[1] Recently, Hanson and Ravishankara reported the heterogeneous hydrolysis of $BrONO_2$ on the sulfuric acid remained large with the hydrolysis probability >0.2.[8] Abbatt showed that HOBr reacted efficiently with HCl and HBr on ice surfaces and on sulfuric acid solutions yielding BrCl and $Br_2$, respectively.[9,10] HOBr may have the ability to activate both bromine and chlorine in the atmosphere and, more importantly, the interhalogen heterogeneous reactions change the partitioning between bromine and chlorine. Ozone destruction by bromine is more efficient than previously estimated without heterogeneous processes. In the regions of the atmosphere where the photolysis of HOBr occurs slowly, such as in the winter at high latitudes, it is reasonable to expect that heterogeneous HOBr chemistry may play a role in understanding ozone depletion.

The main sources for stratospheric bromine species are $CH_3Br$, CBrClF, and $CBrF_3$.[11] HOBr is mainly produced in the atmosphere by the gas-phase reaction of $HO_2$ with BrO and by heterogeneous reactions involving the hydrolysis of $BrONO_2$ on ice clouds (PSCs) and $H_2SO_4$ aerosols in the region of low sunlight or dark.[8,12,13] In the lower stratosphere and the upper troposphere, $BrONO_2$ and HOBr are the main reservoirs for bromine; HCl is the most abundant chlorine reservoir (∼ppb).[2,14] Total inorganic bromine concentration in the lower stratosphere is about 20 ppt.[2] Despite the low concentration of bromine species, the bromine ozone destruction capacity is in part offset by its longer catalytic cycles. Br is approximately 100 times more effective to deplete ozone than that of Cl on a per atom basis in the lower stratosphere.[2,15] Overall, bromine species are responsible for about 25% of polar ozone depletion.[2]

Determining the interaction of HOBr on ice is the essential step toward revealing the reaction mechanism of the HOBr + HCl reaction on type II polar stratospheric cloud and cirrus cloud surfaces. Uptake of HOBr on the ice surface was reported by a couple of groups. Abbatt reported the uptake coefficient $\gamma$ was 0.0017 at 228 K.[9] Allanic et al.[16] reported that $\gamma$ was in the range of 0.11−0.27 at 190 K and 0.05−0.15 at 200 K. The uptake coefficient changes slightly from 190 to 200 K. However, within 30−40 K, the uptake coefficient decreases about 100-fold. It is important to address whether the temperature or the other nature of the uptake process causes this 100-fold change in $\gamma$. This motivated us to examine the nature of the HOBr interaction on the ice film at low temperatures.

The reaction probability for the HOBr + HCl reaction was determined at 190, 200, and 228 K.[9,16] However, the mechanism was not investigated in detail, nor was the BrCl product. The concentration of HOBr and HCl used in these studies was typically in the range of $10^{10}-10^{13}$ molecules/cm$^3$, which is approximately 100-fold higher than found in the lower stratosphere. A common practice is to extrapolate the measured reaction probability to the atmospheric conditions. To perform the extrapolation reliably, one has to determine the reaction mechanism near the atmospheric conditions. This motivated us to investigate the mechanism for the HOBr + HCl reaction.

In this paper, we report the measurements of the uptake coefficient of HOBr on the ice surface and the reaction probability for the reaction of $HOBr + HCl(s) \rightarrow BrCl + H_2O(s)$ on ice surfaces. In the following sections, we will briefly describe the experimental procedures used in the determination of the uptake coefficient and the reaction probability. We will present the results of the uptake coefficient of HOBr on ice as a function of temperature, the thermal desorption of HOBr on ice, and the simulation of HOBr desorption spectra. The reaction probability of the reaction HOBr + HCl is a function of partial HCl pressures and ice film surface temperatures. Finally, we will discuss the nature of the interaction of HOBr with ice and the reaction mechanism for the HOBr + HCl reaction.

## II. Experimental Section

The uptake coefficient, defined as the ratio of the number of molecules lost to the surface to the total number of gas−surface

* Corresponding author. E-mail: lchu@csc.albany.edu.

10.1021/jp991136q CCC: $18.00 
Published on Web 10/07/1999

collisions, of HOBr on the ice surface and the reaction probability measurements were carried out in a flow reactor coupled to a differentially pumped quadrupole mass spectrometer (QMS). The details of the apparatus have been discussed in our previous publications,[17−19] and we will provide a brief description of procedures specifically for this study.

**Flow Reactor.** The cylindrical flow reactor was made of Pyrex glass with an inner diameter of 1.70 cm and a length of 35 cm. The temperature of the reactor was regulated by a liquid nitrogen cooled methanol circulator (Neslab) and measured with a pair of J-type thermocouples located in the middle and at the downstream end of the reactor. During the experiment, the temperature was maintained at a preset level; the stability of the temperature was better than 0.3 K in every experiment. The total pressure of the flow reactor was controlled by a downstream throttle valve (MKS Instrument, model 651C) and was measured by a high-precision Baratron pressure gauge (MKS Instrument, 690A). The stability of the pressure was better than 0.001 Torr. A double capillary Pyrex injector was used to introduce reactants and He−water vapor into the system. To avoid water vapor condensation on the capillary at the low temperature, a room-temperature dry air was passed through the outside of the capillary to keep it warm.

**Ice−Film Preparation.** The ice film was prepared by passing the helium carrier gas into a distilled water bubbler at 293.2 ± 0.1 K. The He−water vapor mixture was then admitted to an inlet of the double capillary injector. The partial water vapor pressure in the reactor was maintained at 0.025−0.2 Torr during the ice deposition. During the course of ice deposition, the injector was slowly pulled out at a constant speed, 2−28 cm/min, and a uniform ice film was deposited on the inner surface of the reactor, which was at the temperature range 190−240 K. The amount of ice−substrate deposited was calculated from the water vapor pressure, the mass flow rate of the helium−water mixture, which was measured by a Hasting mass flow meter, and the deposition time. The average film thickness was calculated by using the geometric area of the flow reactor, the mass of ice, and the bulk density (0.63 g/cm$^3$) of vapor-deposited water ice.[20] For the uptake coefficient measurements, the same thickness of the ice film was used at 190−239 K and the typical film thickness was about 32 $\mu$m. In the reaction probability experiment, the typical average film thickness was about 2.2 $\mu$m at 190 K and 26 $\mu$m at 222 K. The ice film sublimation rate at 222 K was higher than that at 190 K.[21] The loss of the ice film due to the evacuation in the flow reactor was larger. Along with the higher total pressure in the reactor, we had to prepare a thicker film so that the film loss was a minimum. During the experiment, an additional water vapor that is nearly in equilibrium with the vapor pressure of ice was added to compensate the loss of ice.

**HCl−He Mixtures.** HCl−He mixtures were prepared by mixing HCl (Matheson, 99.995%) and helium (Praxair, 99.9995%) in an all-glass manifold, which had been previously evacuated to ∼10 $^{-6}$ Torr. The typical HCl-to-helium mixing ratio was $10^{-3}$ to $10^{-5}$. HCl along with additional helium carrier gas was introduced into the flow reactor via a stainless steel mass flow controller (Teledyne-Hastings), FEP tubing, and the double capillary injector. All transfer lines were passivated by the HCl−He mixture prior to the measurements. The HCl concentration at the end of the injector was monitored by the QMS to ensure the mixture was not lost to the wall of tubings.

**HOBr Preparation and Calibration.** The HOBr solution was prepared by adding bromine (Aldrich, 99.5%) in successive portions to a mixture of 100 mL of ice-cooled 0.5 N sulfuric acid and 3.9 g of silver sulfate in a glass flask until the orange color of excess bromine persisted after continued stirring.[22] After the solution settled in the glass flask for about 10 min, the liquid was decanted into a separatory funnel. The solution was freed from molecular bromine by successive extractions with carbon tetrachloride at 0 °C. The heavier $CCl_4$ phase containing $Br_2$ was removed from the separatory funnel. The interface between the solution and $CCl_4$ was also removed so that all AgBr precipitates were removed from the solution. A slightly yellowish clear HOBr solution was obtained and kept at about 0 °C.

HOBr vapor was bubbled into the movable injector by the helium gas through the FEP tubing and Teflon swagelok. The flow rate was controlled by a Monel metering valve which was treated by the Halocarbon grease.

In HOBr calibration experiments, we deposited an ice film on the inner wall of the flow reactor at 190 K. High concentration HOBr (∼$2 \times 10^{-6}$ Torr) was admitted into the flow reactor and the entire ice surface was exposed to HOBr for about 20 min. HCl ($8 \times 10^{-7}$ Torr) was introduced into the flow reactor and reacted with HOBr to produce BrCl. In this case, HOBr was in excess. Assuming the reaction followed the stoichiometric ratio, the loss of one HCl molecule was equal to form one BrCl molecule. We determined the signal ratio of HCl to BrCl. The other experiment was to have HCl ($3 \times 10^{-6}$ Torr) in excess and repeat the same measurements. In this case, the loss of HOBr molecules (∼$5 \times 10^{-7}$ Torr) was equal to the formation of BrCl molecules. We measured the signal ratio of HOBr to BrCl. From these two experiments, we determined the ratio of the HOBr signal (counts) to HCl signal (counts). These experiments were conducted at different QMS multiplier voltages. The ratio was a constant at a slightly different QMS multiplier voltage provided the ionization voltage and emission current were constant. Knowing both the signal ratio of HOBr to HCl and the HCl concentration, we calculated the HOBr concentration.

**Determination of the Uptake Coefficient.** The uptake coefficient of HOBr on the ice film was determined as follows. First, a fresh ice film was deposited on the inner wall of the flow reactor as described above for every measurement. Second, the helium carrier gas was bubbled through the HOBr solution that was at 273 K. Helium saturated with HOBr vapor was then admitted to an inlet of the double capillary injector. Before the uptake, HOBr was not exposed to the ice surface; an initial HOBr signal was measured. During the uptake coefficient measurement, the sliding injector was pulled out 1 cm at a time. Gas-phase HOBr was taken by the fresh ice surface. The loss of HOBr was monitored at $m/e^- = 96$ by the QMS. The data acquisition time was typically 5−30 s per data point. During this time period, the ice surface was not saturated by HOBr. The loss of gas-phase HOBr was measured as a function of the injector position $z$ (Figure 1). The decay of gas-phase HOBr followed the first-order reaction

$$\ln[\mathrm{HOBr}]_z = -k_s(z/v) + \ln[\mathrm{HOBr}]_0 \qquad (1)$$

where $[\mathrm{HOBr}]_z$ is the gas-phase HOBr concentration at the position $z$ and 0 is the reference injector position. $v$ is the average flow velocity. $\ln[\mathrm{HOBr}]_z$ was plotted versus the uptake time $t = z/v$. The first-order decay rate constant, $k_s$, was calculated from the slope of the least-squares fit to the experimental data. A typical experimental result is shown in Figure 1. The gas-phase diffusion correction for $k_s$ was made using a standard procedure.[23] The corrected rate, $k_g$, was then determined. A HOBr diffusion coefficient of 270 Torr (cm$^2$/s) at 228 K was used in the calculation, and the temperature effect was corrected

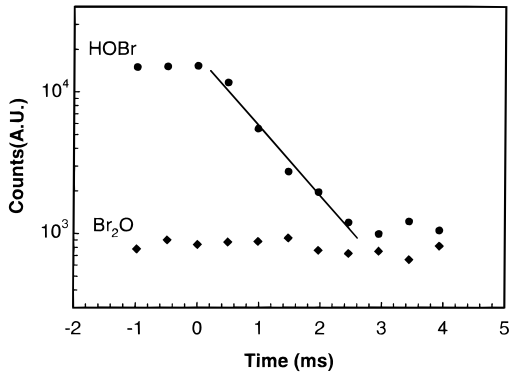


**Figure 1.** The uptake of HOBr on water−ice at $P_{HOBr} = 1.1 \times 10^{-6}$ Torr and 190 K. (●) represents the HOBr signal. The uptake coefficient $\gamma_g = 0.11$. A $Br_2O$ signal (◆) is also shown in the figure. The $Br_2O$ signal was almost unchanged during the HOBr uptake process. This indicated that no HOBr dissociation ($2HOBr \rightarrow Br_2O + H_2O$) was observed during the uptake.

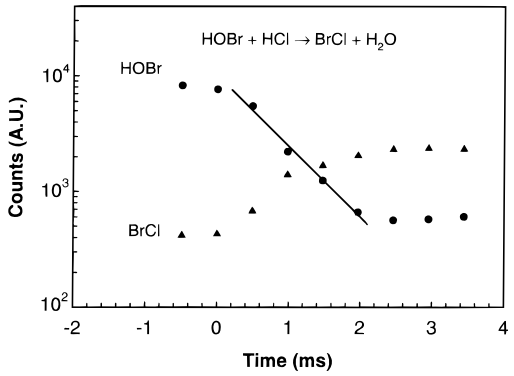


**Figure 2.** Plot of HOBr signal versus the reaction time at 190 K. The pseudo-first-order rate constant $k_s = 9.69 \times 10^2$ s$^{-1}$, and the corrected rate constant $k_g = 1.73 \times 10^3$ s$^{-1}$ as determined from the HOBr decay. The reaction probability $\gamma_g = 0.134$. The total pressure was 0.401 Torr, and the flow velocity was 19.8 m/s. The product BrCl is also shown in the figure.

by $T^{1.75}$.[9] On the basis of the geometric area of the flow-tube reactor, the initial uptake coefficient, $\gamma_g$, was then calculated by using the following equation:

$$\gamma_g = 2Rk_g/(\omega + Rk_g) \tag{2}$$

where $R$ is the radius of the flow reactor (0.85 cm) and $\omega$ is the average molecular velocity for HOBr. A layered pore diffusion model was employed to correct the ice surface roughness in order to obtain the "true" reaction probability $\gamma_t$.[24−27] On the basis of previous studies which were conducted at nearly identical conditions,[20,25,28] $H_2O$ ice films can be approximated as the hexagonally close-packed (hcp) spherical granule stacked in layers.[25] The "true" reaction probability, $\gamma_t$, is related to the value $\gamma_g$ by

$$\gamma_t = \frac{\sqrt{3}\gamma_g}{\pi\{1 + \eta[2(N_L - 1) + (3/2)^{1/2}]\}} \tag{3}$$

where $\eta$ is the effectiveness factor and $N_L$ is the number of granule layers.[29]

**Determination of the Reaction Probability.** The reaction probability of the HOBr + HCl reaction on the ice film was determined in a similar fashion as the uptake coefficient measurement. For every measurement, a fresh ice film was prepared. After the preparation of the ice film, the film surface was saturated by HCl at pressures between $1.3 \times 10^{-7}$ and $1.5 \times 10^{-5}$ Torr. The saturation was monitored by the QMS. With the continuing HCl flow at the same $P_{HCl}$, HOBr was then admitted to the reactor through a separated capillary of the injector. The gas-phase loss of HOBr and the formation of BrCl were measured as a function of the injector position z. A typical experimental result is shown in Figure 2. The pseudo-first-order rate constant $k_s$ was calculated from eq 1. By the same token, the gas-phase diffusion correction was applied and $\gamma_g$ was computed from eq 2.

**HOBr Thermal Desorption Experiment.** The desorption temperature of HOBr on the ice surface was determined using the temperature-programmed desorption (TPD) technique. In this experiment, ice was deposited on the wall of the flow reactor at 188 K and the injector was kept at the upstream end after ice deposition. HOBr was admitted into the flow reactor and exposed to the entire ice surface. The HOBr exposure time was varied from 5 to 30 min to prepare different surface coverage. The ice film was not saturated under this condition. With the HOBr flow off, we ramped the temperature of the flow reactor at ~3 K/min and monitored the gas-phase HOBr molecule by the QMS. At a specific temperature, HOBr started to desorb from the ice surface and then the gas-phase HOBr signal reached a maximum. The desorption temperature is the temperature at which the gas-phase HOBr signal reached the maximum (HOBr peak temperature).

### III. Simulation of the TPD

Molecular dynamic simulations are often used to discover the nature of gas−surface interactions.[30−32] For HOBr on the ice surface, little is known about the gas−surface interaction potential.[33] We chose kinetic simulation to reveal the nature of desorption behavior. A simple kinetic desorption calculation starts with a basic premise that the rate of a simple desorption process

$$A_{ad} \rightarrow A(g) \tag{4}$$

can be written as a configuration average of the rate on each site. In this approximation,

$$\frac{r_d}{N_s} = \sum_j k_j\theta_j \tag{5}$$

where $r_d$ is the overall rate of desorption, $k_j$ is the rate constant for desorption from a site with $j$ nearest neighbors, and $\theta_j = N_j/N_s$ where $N_s$ is the total number of sites available to hold gas moleclules. $N_j$ is the number of occupied sites with $j$ nearest neighbor sites occupied. $k_j$ at each site can be written as

$$k_j = k_0 \exp\left(-\frac{E_d^j}{kT}\right) \tag{6}$$

We assume that the activation energy $E_d^j$ from a given site varies only with the number of nearest neighbors. The preexponential factor $k_0$ is constant. In the TPD experiment, the temperature $T$ varies linearly with the time $t$, $T = T_0 + \beta_H t$, where $\beta_H$ is the heating rate. Equation 5 can be written as

$$\frac{r_d}{N_s} = -\beta_H\left(\frac{d\theta}{dT}\right) = -\beta_H \sum_j\left(\frac{d\theta_j}{dT}\right) = \sum_j k_j\theta_j \tag{7}$$

where $\theta = \Sigma\theta_j$ is the surface coverage. For example, each site on a square lattice can have zero, one, two, three, and four

nearest neighbor sites occupied. Combining eq 6 with eq 7, the rate of desorption is[34]

$$\frac{r_d}{N_s} = -\beta_H\left(\frac{d\theta}{dT}\right) = \sum_j k_0\theta_j \exp\left(-\frac{E_d + \gamma_P jh}{kT}\right) \qquad (8)$$

where $E_d^j = E_d + \gamma_P jh$ is the activation energy for desorption when an adsorbate is surrounded by $j$ nearest neighbors. $E_d$ is also a function of the free energy of an adsorbed molecule $H_1$. $h$ is the interaction energy between two nearest neighbor molecules. $\gamma_P$ is the so-called transfer coefficient. $\gamma_P$ is a measure of the asymmetry of the transition state. $\gamma_P = 0.5$ means the potential surface is symmetric at the transition state. If $\gamma_P \approx 1$, the transition state is like the product. Equation 8 is straightforward to solve with the exception of $\theta_j$ which is a function of both $H_1$ and $h$. A number of approximation methods such as Bragg−William and Bethe−Peireles can be used to calculate $\theta_j$.[34−36] In this study, we used the lattice gas/Monte Carlo (MC) simulation approach to compute $\theta_j$. The reasons are that the MC simulation considers both the adsorbate−surface and lateral interactions. The simulation provides information on both the gas−surface interaction and adsorbent−adsorbent interactions. This method was successful in predicting the order−disorder and surface phase transition where the Bragg−William method failed.[34,36,37] Since we know so little about the HOBr/ice system (also see the results section),[33] it is reasonable to employ a general approach to compute $\theta_j$.

The partition function of the system and the ensemble averaged coverage $\theta_j$ as a function of $H_1$ and $h$ were computed in a simulation.[34,36,37] The HOBr molecule was treated as a single particle (associative chemisorption) in the simulation. A 40 × 40 periodic surface site, $n_{site}$, was employed in the calculation. A Fortran code developed in our laboratory was used to carry out these calculations. It utilized 4000 steps to randomize the occupancy matrix, and the coverage was calculated by averaging over a million Monte Carlo steps $n_{step}$.

$$\theta_j = \frac{1}{n_{step}}\sum_{steps} n_j/n_{site} \qquad (9)$$

where $n_j$ is the number of adsorbed HOBr molecules with $j$ nearest neighbor sites occupied at the end of a simulation.

## IV. Results

**Uptake Coefficient of HOBr on Ice Surfaces.** A typical uptake experimental result is shown in Figure 1. The initial uptake coefficient ($\gamma_g$) of HOBr on the fresh ice film was determined as a function of the temperature from 190 to 239 K, and the result is shown in Figure 3. The "true" uptake coefficient $\gamma_t$ and detailed experimental conditions are tabulated in Table 1. Both $k_s$ and $\gamma_g$ were a mean value of 2−6 measurements. The error bars listed in the table and Figure 3 include both one standard deviation ($\pm\sigma$) of the mean value and the standard deviation of the least-squares fit of $k_s$ shown in Figure 1. $\gamma_t$ was computed from $\gamma_g$ based on the pore diffusion model, i.e., eq 3.[25] Keyser et al.[25] used a tortuosity factor of 4 in the treatment of ice films at 202 K, and the same factor was chosen to use in this calculation. In the temperature range 190−218 K, log $\gamma_g$ decreased with $1/T$. The solid line in Figure 3 is the least-squares fit of the data in the range 190−218 K. It can be expressed in an Arrhenius type expression as $\gamma_g = (2.2 \pm 0.8) \times 10^{-10} \exp((3809 \pm 76)/T)$. The uptake coefficient decreased dramatically, about 10-fold, from 218 to 223 K. The plot shows a "discontinuity" in this temperature range. At the temperature range 223−239 K, the uptake coefficient was substantially lower than the expected value of the solid line. log $\gamma_g$ still seemed linear with $1/T$ in this narrow temperature range. The slope of the dashed line was slightly different from that of the solid line. $\gamma_g$ in this temperature range can be expressed as $\gamma_g = (1.8 \pm 3.6) \times 10^{-12} \exp((4658 \pm 456)/T)$. The nature of this observation will be discussed in a later section.

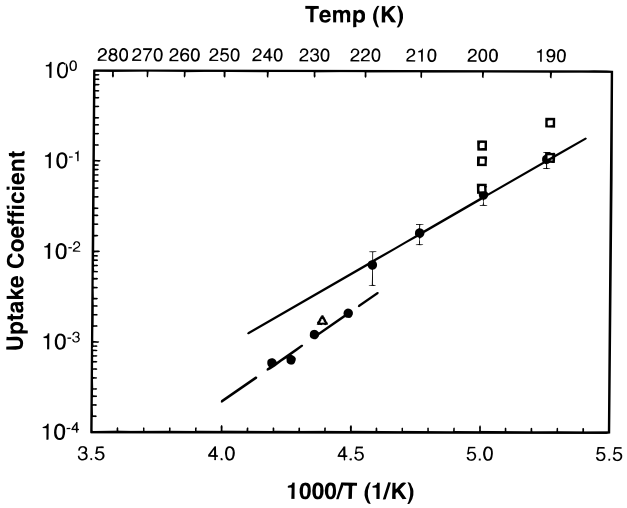


**Figure 3.** Plot of the HOBr uptake coefficient on the ice surface versus $1/T$. The solid line is the least-squares fit to the experimental data at 190−218 K. The dashed line is the least-squares fit to the experimental data at 223−239 K. The total pressure was 0.50 Torr and $P_{HOBr} = 1.1 \times 10^{-6}$ Torr. (□) represents the results of Allanic et al.; (△) is the result of Abbatt. See text for details.

HOBr, $Br_2O$, and $Br_2$ were monitored by the QMS in some experiments. Figure 1 shows that no $Br_2O$ ($m/e^- = 174$) was detected from the reaction of $2HOBr \rightarrow Br_2O + H_2O$. Also, no net $Br_2$ signal ($m/e^- = 158, 160$) change was observed during the uptake. This suggests that the HOBr loss process might not involve surface reactions. The same conclusion was derived by Allanic et al.[16]

**Uptake of HOBr on Ice.** The uptake amount of HOBr on ice surfaces was measured at 198, 204, and 209 K at different

**TABLE 1: Uptake Coefficient of HOBr on Ice Films**[a]

| temperature (K) | thickness ($\mu$m) | $v$ (m/s) | $P_{total}$ (Torr) | $k_s$ (1/s) | $k_g$ (1/s) | $\gamma_g$ | $\gamma_t$ |
|---|---|---|---|---|---|---|---|
| 190.5 ± 0.8 | 31.5 | 29.6 | 0.27 | 950 ± 119 | 1337 | 0.11 ± 0.03 | 0.03 |
| 199.8 ± 0.6 | 31.9 | 21.1 | 0.40 | 435 ± 117 | 533 | 0.04 ± 0.02 | $7.2 \times 10^{-3}$ |
| 210.1 ± 0.3 | 30.6 | 19.4 | 0.50 | 185 ± 61 | 203 | 0.02 ± 0.01 | $2.6 \times 10^{-3}$ |
| 218.4 ± 0.5 | 32.0 | 18.6 | 0.50 | 90.0 ± 57 | 94 | $(7.1 \pm 3.5) \times 10^{-3}$ | $4.4 \times 10^{-4}$ |
| 222.9 ± 0.3 | 30.7 | 19.0 | 0.50 | 26.6 ± 0.9 | 26.9 | $(2.1 \pm 0.5) \times 10^{-3}$ | $5.6 \times 10^{-5}$ |
| 229.6 ± 0.9 | 32.5 | 2.4 | 2.00 | 15.1 ± 1.5 | 15.9 | $(1.2 \pm 0.4) \times 10^{-3}$ | $2.6 \times 10^{-5}$ |
| 234.4 ± 0.3 | 32.6 | 2.5 | 2.00 | 8.2 ± 1.4 | 8.41 | $(6.3 \pm 1.9) \times 10^{-4}$ | $1.2 \times 10^{-5}$ |
| 238.6 ± 0.5 | 32.3 | 2.5 | 2.00 | 7.6 ± 5.0 | 7.81 | $(5.8 \pm 3.4) \times 10^{-4}$ | $1.1 \times 10^{-5}$ |

[a] Average film thickness was 32 ± 2 $\mu$m. $P_{HOBr} = (1.1 \pm 0.8) \times 10^{-6}$ Torr. $\gamma_t$ was calculated from eq 3 by using $N_L = 16$. $\eta$ was computed using the tortuosity factor $\tau = 4$ and true density $\rho_t = 0.925$ g/cm$^3$ at the $N_L = 16$ conditions. See text and ref 25 for details.

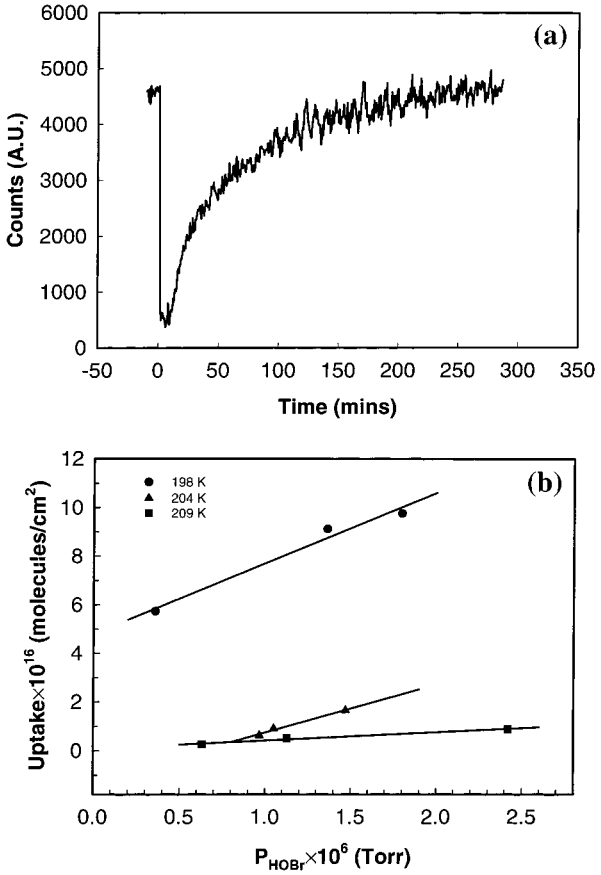


**Figure 4.** (a) Plot of the HOBr signal versus the time for the HOBr uptake on water−ice at $P_{HOBr} = 1.1 \times 10^{-6}$ and 198 K. The uptake started at $t = 0$ min when HOBr exposed to the entire ice film. It took about 250 min to saturate the film. (b) Plot of the surface density ($\theta$) versus the partial HOBr pressures for the HOBr uptake on the ice surface at 198, 204, and 209 K, respectively. The film thickness was $32 \pm 2$ $\mu$m. The solid lines are the fit to the equation $\theta = K_P P$.

$P_{HOBr}$. In these experiments, we determined the total amount of HOBr lost to ice until the surface was saturated. The gas-phase HOBr loss was recorded as a function of the real uptake time and the experimental procedure was identical to previous publications.[17,26,38] Figure 4a is a typical plot of the HOBr signal versus the time on water−ice at 198 K. The uptake started at $t = 0$ min when HOBr exposed to the entire ice film (150 cm$^2$). It took about 250 min to saturate the entire ice surface. Figure 4b is a plot of the uptake amount, expressed as the surface density ($\theta$) per unit area, versus the partial HOBr pressures for the HOBr uptake on the ice surface at 198, 204, and 209 K, respectively. The solid lines are the fit to the isotherm $\theta = K_P P$. $K_P$ were determined to be $2.9 \times 10^{22}$, $2.0 \times 10^{22}$, and $3.4 \times 10^{21}$ molecules/(Torr cm$^2$) at 198, 204, and 209 K, respectively. The uptake amount per unit geometric surface area was comparable with HBr and HI.[17,38]

**Desorption Temperature of HOBr on Ice.** The thermal desorption of HOBr from the ice film at the different surface exposures is shown in Figure 5. The solid lines are HOBr thermal desorption profile from experimental measurements. HOBr molecules were exposed onto the ice surface at 188 K. HOBr exposure time varied up to 30 min. The ice surface was not saturated by the HOBr molecule within 30 min at 188 K. On the basis of the uptake experiment, it takes about 3−4 h to saturate the surface (cf. Figure 4a). With the HOBr flow turned off, HOBr molecules did not desorb from surface at 188 K. When we increased the ice film temperature, HOBr desorbed from the ice surface at $T_d = 214$, 220, 225, and 229 K with the exposure time of 5, 10, 20, and 30 min, respectively. The uncertainty in the temperature measurement was about ±1.5 K. The exposure amount as monitored by the QMS was converted to the coverage. They are equivalent to 0.064, 0.13, 0.26, and 0.39 ML, respectively. The coverage was estimated from the total exposure amount and the size of HOBr, 19.5 Å$^2$ (van der Waals radius).[39] Further, we assumed that all HOBr molecules remained on the surface and the total available surface area was the same as the geometric area of the film. It is interesting to note that the desorption temperature was about the same as the "discontinuity" in $\gamma_g$ at 218−223 K.

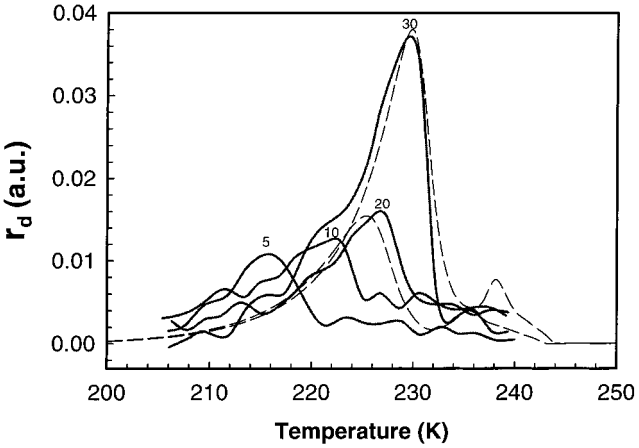


**Figure 5.** Thermal desorption spectra (solid lines) of HOBr from the ice film with different surface exposure times as indicated in the figure. The desorption temperature increased from 214, 220, 225, to 229 K as the exposure increased from 0.064, 0.13, 0.26, to 0.39 ML, respectively. For the illustration purpose, the dashed lines with parameters $E_d = 15.8 \pm 2$ kcal/mol, $h = 0.69 \pm 0.15$ kcal/mol, $k_0 = 7 \times 10^{12\pm2}$, and $\gamma_p = 1$ are based on the TPD simulation. See text for details.

**TABLE 2: Parameters Used in the TPD Simulation**

| $\gamma_p$ | $E_d$ (kcal/mol) | $h$ (kcal/mol) | $k_0$ (1/s) |
|---|---|---|---|
| 0.35 | $17.1 \pm 2$ | $0.72 \pm 0.15$ | $7 \times 10^{13\pm2}$ |
| 0.5 | $16.0 \pm 2$ | $0.72 \pm 0.15$ | $7 \times 10^{12\pm2}$ |
| 1.0 | $15.8 \pm 2$ | $0.69 \pm 0.15$ | $7 \times 10^{12\pm2}$ |

Figure 5 shows that the desorption temperature $T_d$ is shifted to a high temperature when the exposure increases. This observation cannot be explained by the first-order desorption kinetics in which $T_d$ is independent of $\theta$.[34] To reveal the nature of the desorption process, the desorption spectra were simulated on the basis of eq 8 and as outlined in the previous section. The thermal desorption profile obtained from the simulation was shown in Figure 5 as dash lines. For the purpose of clear illustration, only two simulation plots were shown in the figure. The simulated spectra were matched to the experimental spectra both in the peak position and full-width at half-maximum simultaneously by adjusting parameters $E_d$, $h$, and $k_0$ at different $\gamma_p$. The results were tabulated in Table 2. The results showed that the parameter $\gamma_p$ is not very sensitive to the simulated TPD spectra. With $h > 0$, the simulation suggests that the adsorbed HOBr molecules exhibited an attractive interaction between them on the surface and tended to form HOBr "islands" at a higher coverage on the surface. The "extra" thermal energy was required to break the attractive interaction and desorb the molecule to the gas phase. This is the key to understanding the desorption temperature as a function of the exposure.

**HOBr + HCl → BrCl + $H_2O$.** The reaction probability for HOBr + HCl(s) → BrCl + $H_2O$(s) was determined by observing both the decay of gas-phase HOBr, monitored at $m/e^- = 96$, and the formation of gas-phase BrCl, monitored at $m/e^- = 114$,

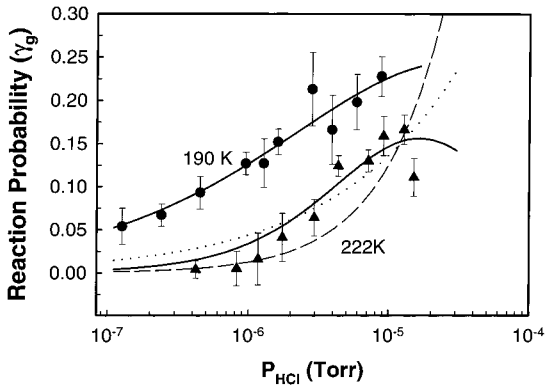


**Figure 6.** Plot of the reaction probability versus the partial HCl pressure for the reaction HOBr + HCl(s) → BrCl + $H_2O$(s) on ice at 190 and 222 K. The total pressure in the reactor was 0.401 Torr at 190 K. The solid line was fitted to a Langmuir−Hinshelwood type mechanism where HCl was dissociatively adsorbed on the surface at 190 K. At 222 K, the total pressure was 0.501 Torr. The dashed line was fitted to a Eley−Rideal mechanism and the solid line was fitted to a Langmuir−Hinshelwood mechanism.

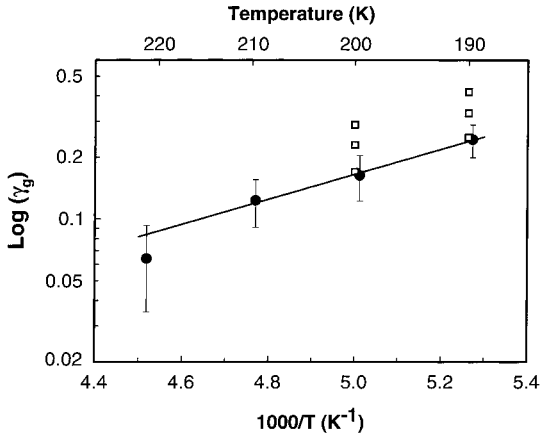


**Figure 7.** Plot of the reaction probability versus 1/*T*. The solid line is the least-squares fit to the experimental data. The total pressure was 0.501 Torr. $P_{HOBr} = 1.9 \times 10^{-6}$ Torr and $P_{HCl} = 2.6 \times 10^{-6}$ Torr. (□) represents the results of Allanic et al.

as a function of injection position (see Figure 2). The concentration of HCl used in this study was always greater than that of HOBr, and the ice surface was saturated by HCl prior to the reaction; thus, the pseudo-first-order reaction condition was valid. The reaction probability $\gamma_g$ as a function of $P_{HCl}$ at 190 K and 222 K is presented in Figure 6. The detailed experimental conditions and the "true" reaction probability are listed in Table 3. The tabulated $k_s$ and $k_g$ were measured from the HOBr loss over the surface. The error bars included one standard deviation of the mean value and the uncertainty of $k_s$ as determined from the least-squares fit. Figure 6 indicates that the reaction probability increases as $P_{HCl}$ increases and becomes less pressure dependent at $P_{HCl} > 3 \times 10^{-6}$ Torr. At a warmer temperature, 222 K, $\gamma_g$ is in the range of 0.004 to 0.19 and showed a similar temperature-dependent trend as the lower temperature data. However, the reaction probability at 222 K is lower than that at 190 K.

The reaction product, BrCl, was measured at its parent peak $m/e^- = 114$. The formation of BrCl is shown in Figure 2. $\gamma_g$ determined from the formation of BrCl is nearly identical to that from the loss of HOBr over the ice as shown in Table 3.

The reaction probability was also measured at 190, 200, 210, and 221 K. The same thickness, ~28 $\mu$m, of the ice film was used in these experiments. The result is shown in Figure 7. The detailed experimental results are listed in Table 4. The results show that the reaction probability decreased as the temperature increased from 190 to 221 K. The reaction probability can be expressed as $\gamma_g = (1.5 \pm 0.8) \times 10^{-4} \exp((1406 \pm 105)/T)$.

## IV. Discussion

**Uptake Coefficient of HOBr on Ice Surfaces.** The variation of the uptake coefficient with the temperature and coverage can be discussed in terms of a precursor moderated adsorption model.[34,40,41] In this model, molecules impinge onto a weakly bound state, called the precursor state, then molecules can diffuse around the surface to find a site to adsorb. The reason we attempt to employ this model is as follows. Figure 4a showed the uptake as a function of the time and it implied that the uptake coefficient was nearly a constant at the lower coverage (the

**TABLE 3: Reaction Probability for the Reaction of HOBr + HCl(s) → BrCl + $H_2O$(s) on Ice Films at Different Pressures[a]**

| $T$ (K) | $P_{HCl}$ (Torr) | $v$ (m/s) | $k_s$ (1/s) | $k_g$ (1/s) | $\gamma_{g(HOBr)}$ | $\gamma_{g(BrCl)}$ | $\gamma_t$ |
|---|---|---|---|---|---|---|---|
| 189.5 ± 0.3 | $1.27 \times 10^{-7}$ | 19.0 | 499 ± 76 | 650 | 0.05 ± 0.01 | 0.07 ± 0.01 | 0.01 |
| 189.2 ± 0.4 | $2.40 \times 10^{-7}$ | 19.1 | 634 ± 123 | 843 | 0.07 ± 0.01 | 0.09 ± 0.01 | 0.02 |
| 188.9 ± 0.3 | $4.51 \times 10^{-7}$ | 19.3 | 704 ± 103 | 1040 | 0.09 ± 0.01 | 0.07 ± 0.004 | 0.02 |
| 189.0 ± 0.8 | $9.50 \times 10^{-7}$ | 19.4 | 908 ± 60 | 1617 | 0.13 ± 0.01 | 0.09 ± 0.01 | 0.04 |
| 189.9 ± 0.6 | $1.28 \times 10^{-6}$ | 20.0 | 913 ± 368 | 1630 | 0.13 ± 0.05 | 0.08 ± 0.01 | 0.04 |
| 189.4 ± 0.3 | $1.61 \times 10^{-6}$ | 19.1 | 1030 ± 141 | 1970 | 0.15 ± 0.02 | 0.16 ± 0.02 | 0.05 |
| 190.3 ± 1.0 | $2.82 \times 10^{-6}$ | 20.0 | 1230 ± 238 | 2860 | 0.21 ± 0.04 | 0.11 ± 0.02 | 0.07 |
| 189.3 ± 1.1 | $3.92 \times 10^{-6}$ | 20.6 | 1050 ± 431 | 2100 | 0.17 ± 0.07 | 0.09 ± 0.01 | 0.05 |
| 190.8 ± 0.5 | $5.86 \times 10^{-6}$ | 19.9 | 1200 ± 165 | 2650 | 0.20 ± 0.03 | 0.17 ± 0.03 | 0.07 |
| 189.4 ± 0.3 | $8.77 \times 10^{-6}$ | 20.3 | 1290 ± 102 | 3400 | 0.23 ± 0.02 | 0.19 ± 0.04 | 0.08 |
| 221.6 ± 0.3 | $4.22 \times 10^{-7}$ | 18.0 | 48.9 ± 8.1 | 50.1 | 0.004 ± 0.001 | 0.005 ± 0.001 | 0.0002 |
| 221.8 ± 0.3 | $8.23 \times 10^{-7}$ | 17.5 | 65.6 ± 12.6 | 67.7 | 0.005 ± 0.002 | 0.005 ± 0.001 | 0.0002 |
| 221.7 ± 0.3 | $1.17 \times 10^{-6}$ | 18.2 | 191 ± 34 | 210 | 0.016 ± 0.002 | 0.032 ± 0.006 | 0.002 |
| 221.2 ± 0.6 | $1.74 \times 10^{-6}$ | 18.3 | 163 ± 90 | 177 | 0.014 ± 0.005 | 0.008 ± 0.002 | 0.001 |
| 221.3 ± 0.3 | $2.94 \times 10^{-6}$ | 18.7 | 564 ± 416 | 774 | 0.064 ± 0.029 | 0.094 ± 0.015 | 0.015 |
| 221.6 ± 0.3 | $4.35 \times 10^{-6}$ | 18.7 | 966 ± 90 | 1710 | 0.124 ± 0.011 | 0.100 ± 0.020 | 0.037 |
| 222.7 ± 0.3 | $7.13 \times 10^{-6}$ | 18.8 | 998 ± 150 | 1800 | 0.130 ± 0.018 | 0.200 ± 0.040 | 0.039 |
| 221.5 ± 0.5 | $9.14 \times 10^{-6}$ | 18.6 | 1070 ± 222 | 2190 | 0.193 ± 0.091 | 0.189 ± 0.048 | 0.064 |
| 221.7 ± 0.3 | $1.28 \times 10^{-5}$ | 18.6 | 1140 ± 178 | 2350 | 0.166 ± 0.025 | 0.146 ± 0.029 | 0.053 |
| 221.3 ± 0.3 | $1.51 \times 10^{-5}$ | 18.6 | 898 ± 139 | 1580 | 0.111 ± 0.017 | 0.060 ± 0.025 | 0.032 |

[a] Mean total pressure was 0.401 ± 0.001 Torr at 189.5 K and 0.501 ± 0.001 Torr at 221.7 K. Average ice film thickness was 2.2 ± 0.2 $\mu$m at 189.5 K and 26 ± 3 $\mu$m at 221.7 K. $\gamma_t$ was calculated using eq 3 and the tortuosity factor of 4.[25] $N_L = 5$ and 15 for the thin and thick film, respectively. $P_{HOBr} = (1.1 \pm 0.8) \times 10^{-6}$ Torr when $P_{HCl}$ was in the range of $1.3 \times 10^{-6}$ to $8.8 \times 10^{-6}$ Torr. $P_{HOBr} = (1.0 \pm 0.5) \times 10^{-7}$ Torr when $P_{HCl}$ was in the range of $1.3 \times 10^{-7}$ to $1.2 \times 10^{-6}$ Torr.

**TABLE 4: Reaction Probability for the Reaction of HOBr + HCl(s) → BrCl + $H_2O$(s) on Ice Films at Different Temperatures[a]**

| temperature (K) | 1000/$T$ (1/K) | $v$ (m/s) | $k_s$ (1/s) | $k_g$ (1/s) | $\gamma_g$ | $\gamma_t$ |
|---|---|---|---|---|---|---|
| 189.7 ± 0.4 | 5.273 | 15.9 | (1.15 ± 0.01) × $10^3$ | 3.32 × $10^3$ | 0.24 ± 0.04 | 0.08 |
| 199.6 ± 0.5 | 5.011 | 16.5 | (1.01 ± 0.07) × $10^3$ | 2.18 × $10^3$ | 0.16 ± 0.04 | 0.05 |
| 209.7 ± 0.3 | 4.770 | 17.3 | (9.10 ± 0.49) × $10^2$ | 1.65 × $10^3$ | 0.12 ± 0.03 | 0.04 |
| 221.3 ± 0.3 | 4.519 | 18.7 | (5.64 ± 1.57) × $10^2$ | 7.74 × $10^2$ | 0.06 ± 0.03 | 0.01 |

[a] Mean total pressure was 0.501 ± 0.001 Torr. Mean ice film thickness of 28.3 ± 1.7 $\mu$m and $N_L$ = 15 were used in calculating $\gamma_t$. $P_{HCl}$ = (2.63 ± 0.21) × $10^{-6}$ Torr. $P_{HOBr}$ = (1.86 ± 0.22) × $10^{-6}$ Torr.

HOBr amount loss onto ice was about the same at $t \approx 0-10$ min) and then slowly decreased to zero at the saturation coverage. This trend cannot be explained by the Langmuir model, which assumes the adsorbate binds to a series of identical surface sites. The Langmuir adsorption law predicts that the uptake coefficient varies linearly with the coverage. With the precursor model, we may picture the uptake process as follows. Below the desorption temperature, HOBr molecules trap onto the precursor state with a high probability and then migrate to the adsorption state. Above the desorption temperature, HOBr molecules trapped onto the precursor state would be easily desorbed simply because the thermal energy may overcome the barrier, but a small fraction of HOBr molecules may still adsorb on the adsorption state with finite residence time. The precursor model can be summarized by the following equations:

$$\mathrm{HOBr(g)} \underset{k_2}{\overset{k_1}{\rightleftharpoons}} \mathrm{HOBr(p)} \tag{10}$$

$$\mathrm{HOBr(p)} \xrightarrow{k_3} \mathrm{HOBr\ (ad)} \tag{11}$$

Reaction 10 represents the gas-phase HOBr molecules trapped onto and out of the precursor state. Reaction 11 represents the migration of HOBr from the precursor to the adsorption site. The net gas-phase HOBr loss rate below the desorption temperature is

$$\mathrm{Rate} = k_1[\mathrm{HOBr(g)}] - k_2[\mathrm{HOBr(p)}] \tag{12}$$

[HOBr(p)] can be calculated from the steady-state approximation,

$$\gamma = \frac{\mathrm{Rate}}{1/4\omega(\mathrm{HOBr(g)})} = \frac{\alpha k_3}{k_2 + k_3} \tag{13}$$

where $\alpha = 4k_1/\omega$ and $\omega$ is the molecular velocity of HOBr

$$\gamma = \frac{\alpha}{1 + k_2/k_3} = \frac{\alpha}{1 + \nu_2/\nu_3 \exp(-(E_2 - E_3)/kT)} \tag{14}$$

where $v_i$ is the pre-exponential factor and $k$ is the Boltzmann constant. The data at 190−218 K were fitted to eq 14 and are shown in Figure 8 as the solid line. Three parameters, $E_2 - E_3$ = 5.6 kcal/mol, $\alpha$ = 0.79, and $\nu_2/\nu_3$ = 1.8 × $10^7$, were determined form the fitting. $E_2$ is the activation energy of molecules from the precursor to the gas phase. $E_3$ is the activation energy of molecules from the precursor to the adsorption state. $E_2 - E_3$ = 5.6 kcal/mol indicates that a precursor molecule easily overcomes the barrier and traps in the adsorption state. It is a nonactivated adsorption process, and the energetics of the system is mainly controlled by the adsorption state.

Since the desorption temperature of HOBr on the ice surface is about 220 K, the precursor state is assumed to be the weakly bound physisorption mobile state. We expect the surface resident time for HOBr in the precursor state is shorter than the experimental time scale (data acquisition time) at $T > T_d$. In another word, HOBr may not remain on the precursor state. A small fraction of HOBr is expected to get onto the adsorption state and the rate of uptake is proportional to the number of HOBr that get onto the adsorption state,

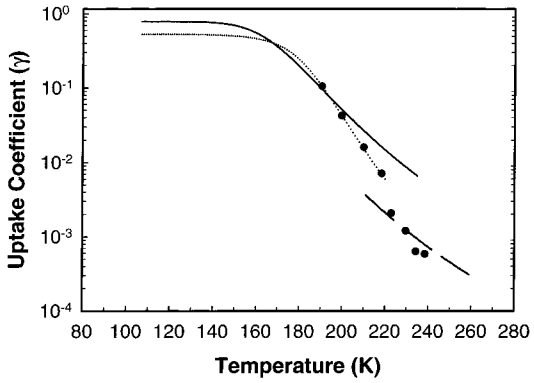


**Figure 8.** Plot of log $\gamma$ versus the temperature for HOBr on the ice surface. The solid line is the least-squares fit to the precursor model at 190−218 K. The dashed line was fitted to the data at 223−239 K. The dotted line is the prediction from a modified precursor model.

$$\mathrm{Rate} = k_3[\mathrm{HOBr(p)}] \tag{15}$$

[HOBr(p)] can be calculated from reaction 10, and eq 15 can be written as

$$\gamma = \frac{\alpha}{k_2/k_3} = \frac{\alpha}{\nu_2/\nu_3 \exp(-(E_2 - E_3)/kT)} \tag{16}$$

The accommodation coefficient, $\alpha$, and activation energies, $E_2$ and $E_3$, are independent of the temperature in this model. The data at 223−239 K are fitted using eq 16 with the constraint of $\alpha$ = 0.79 and $E_2 - E_3$ = 5.6 kcal/mol. $\nu_2/\nu_3$ = 1.3 × $10^8$ is obtained and the fitted curve is shown in Figure 8 as the dashed line. This value, $\nu_2/\nu_3$ = 1.3 × $10^8$, is slightly different from 1.8 × $10^7$ obtained from the lower temperature. It is interesting to note that $E_2 - E_3$ is close to the value obtained from $ClONO_2$ hydrolysis on the ice surface ($E_2 - E_3$ = 4.1 kcal/mol), as is the $\nu_2/\nu_3$ ratio.[42] Berland et al.[42] pointed out that it is possible to have a higher $\nu_2/\nu_3 = 10^7$ ratio for a surface reaction which proceeds through a cyclic transition state. Considering both the simplicity of the model and the uncertainty of the measurement, the agreement at both temperature regions is good. The model predicts that the uptake coefficient will be nearly temperature independent below 160 K and the uptake process will be mainly controlled by the accommodation of HOBr onto the precursor state (see Figure 8). At about 200 K, a competition between $k_2$ and $k_3$ channels results in the uptake coefficient being strongly dependent on the temperature, and eventually $\gamma$ is controlled by $k_3$ above the desorption temperature.

The solid line in Figure 8 does not predict the data very well. We attribute this to the simplicity of the model. The adsorption rate constant $k_3$ may be corrected for the probability of finding free adjacent sites $f(\theta)$. This is a similar concept as the TPD simulation and other models.[43] One of the simplest forms for

*f(θ)* can be $1 - \theta$.[40] Equation 14 becomes

$$\gamma = \frac{\alpha}{1 + \frac{k_2}{k_3(1-\theta)}} \quad (17)$$

Using eq 17, the fitting result is shown in Figure 8 as the dotted line. The model prediction is in excellent agreement with the experimental results.

**Thermal Desorption of HOBr.** The attractive interaction between adsorbed HOBr molecules is believed to be the cause of increases in desorption temperature as the exposure increases. At 190 K, the ice surface is very dynamic.[21,44] $H_2O$ molecules desorb from ice at rates of ~100−1000 BL/s at 200−210 K, and the ice evaporation rate is expected to be affected by the presence of HOBr on the surface.[45] One concern was a possibility that a large amount of HOBr diffused into the bulk of the ice film. In that case, the desorption temperature would really measure the desorption of HOBr from the bulk phase. The more HOBr in the bulk, the higher the temperature (energy) that would be required to desorb HOBr. In a separate experiment, we monitored both HOBr and $H_2O$ signals during the desorption events and found that the desorption temperature for HOBr was several degrees lower than that of $H_2O$. If HOBr was in the bulk, the desorption temperature of HOBr and $H_2O$ would be expected to be identical. It is important to point out when a large amount of HOBr (~1 ML) was dosed onto the ice surface, the desorption of HOBr occurred first (232 K), followed by an $H_2O$ peak (a broad peak started at ~240 K), and finally a second, very small HOBr peak (~260 K, 10% of the first HOBr peak). This suggests that a small fraction of HOBr diffused into the bulk, below the surface dynamic layer, at the higher HOBr exposure condition. At a lower HOBr exposure, the same situation can occur. However, with $\sim 10^3-10^4$ BL/s ice evaporation rate at 220 K,[45] those HOBr molecules that diffused into the bulk may be within the surface dynamic layer as estimated from the Einstein formula $z = \sqrt{Dt} \approx 1\ \mu$m.[46] Thus, the attractive interaction is the main cause of an increase in $T_d$ as the exposure increases.

**Reaction Mechanism.** On the basis of experiments presented here, some conclusion concerning the mechanism of the HOBr + HCl reaction may be drawn. As described in the previous section, the ice film was pretreated by HCl and the surface was saturated. The uptake coefficient of HCl on the ice surface is ~0.3, and this should not be the rate-limiting step.[47] The uptake of HOBr on the water−ice is efficient at the lower temperature (190−200 K), but not fast enough at the warmer temperature as presented in Figure 3. If this is the rate-limiting step of the reaction, then the measured reaction probability is expected to be equal to the rate of the uptake. Clearly this is not the case as presented in Figure 3 and Figure 6. On the basis of the results of the TPD study, we know that both HOBr and HCl were adsorbed on the surface. It is likely that the rate of the reaction is controlled by the adsorbed HOBr and HCl. We may write the mechanism as the Langmuir−Hinshelwood type, it is shown as follows:

$$\mathrm{HCl(g)} + \mathrm{S} \underset{k_2}{\overset{k_1}{\rightleftharpoons}} \mathrm{HCl(ad)} \leftrightarrow \mathrm{H^+(ad)} + \mathrm{Cl^-(ad)} \quad (18)$$

$$\mathrm{HOBr(g)} + \mathrm{S} \underset{k_4}{\overset{k_3}{\rightleftharpoons}} \mathrm{HOBr(ad)} \quad (19)$$

$$\mathrm{HOBr(ad)} + \mathrm{H^+(ad)} + \mathrm{Cl^-(ad)} \xrightarrow{k_s} [\mathrm{HOBr\cdots ClH(ad)}] \rightarrow \mathrm{BrCl(g)} + \mathrm{H_2O(ad)} \quad (20)$$

It is convenient to describe the reaction in terms of the ideal surface reaction *empirically*. This kind of mechanism may provide a simple picture as to how HOBr and HCl molecules react with each other to form products. Since reactions 18 and 19 reached the steady state quickly, reaction 20 is the expected rate-determining step. The rate of the reaction is proportional to the HOBr and HCl surface concentration and can be expressed as the Hougen and Watson rate law,[34,40]

$$R = -\frac{dP_{HOBr}}{dt} = k_s \theta_{HOBr} \theta_{HCl} \quad (21)$$

The reaction probability, $\gamma$, is given by $R/\phi_{HOBr}$, where $\phi_{HOBr} = (P_{HOBr}/\sqrt{2\pi mkT})$ is the flux of HOBr on the surface and $m$ is the molecular weight of HOBr. $\gamma$ can be written as

$$\gamma = \frac{R}{\phi_{HOBr}} = \gamma_o \frac{b_{HOBr} b_{HCl} P_{HCl}^{1/2} S_o}{(1 + b_{HCl} P_{HCl}^{1/2} + b_{HOBr} P_{HOBr})^2} \quad (22)$$

where $b_{HCl} = k_1/k_2$, $b_{HOBr} = k_3/k_4$, $S_o$ is the total surface sites, and $\gamma_o = k_s \sqrt{2\pi mkT}$. $b_{HCl}$ and $b_{HOBr}$ are constant at a given temperature. The term $b_{HCl} P_{HCl}^{1/2}$ represents the HCl molecules dissociatively adsorbed on the ice surface. Equation 22 was used to fit the experimental data at 190 K, and the result is shown in Figure 6 as the solid line. The fitted line matches the experimental results very well. This suggests that the reaction follows the Langmuir−Hinshelwood type at 190 K.

The experimental result at 222 K was also fitted by eq 22, and the result is shown in Figure 6 as the dotted line. The line does not represent the result very well at the higher HCl pressure ($P_{HCl} > 10^{-5}$ Torr). Different expressions for the mechanism were used to perform the fitting procedure for the 220 K data. They are also shown in Figure 6. The dashed line was fitted to the following equation:

$$\gamma = \frac{R}{\phi_{HOBr}} = \gamma_o \frac{b_{HOBr} P_{HCl} S_o}{1 + b_{HOBr} P_{HOBr}} \quad (23)$$

and the solid line was fitted to eq 24,

$$\gamma = \gamma_o \frac{b_{HOBr} b_{HCl} P_{HCl} S_o}{(1 + b_{HCl} P_{HCl} + b_{HOBr} P_{HOBr})^2} \quad (24)$$

Equation 23 was based on the following experimental observation. We determined the desorption temperature of HCl on the ice film is in the range of 210−220 K with $P_{total} = 0.5$ Torr in the flow reactor. This is equivalent to the surface residence time of HCl at 222 K being approximately seconds.[48] HCl may not permanently adsorbed on the surface at the experimental time scale. We can approximately treat the reaction occurred between the gas-phase HCl molecule and adsorbed HOBr. If this is the case, the reaction follows the Eley−Rideal type. $\gamma$ can be written as eq 23. Equation 23 fitted to the data reasonably at $P \lesssim 2 \times 10^{-6}$ Torr; however, it predicted the reaction probability to diverge at $P_{HCl} > 10^{-5}$ Torr. Overall, this reaction does not seem represented by the Eley−Rideal mechanism very well.

Equation 24 is a brutal force approach. HCl molecules adsorb on the surface with a short surface residence time at 222 K or hop across the ice surface.[49] The complete solvation/ionization of HCl on the ice surface requires several $H_2O$ molecules to surround an HCl molecule and proton transfer from HCl to a water molecule.[50] HCl would not be ionized in the ice bulk phase, and the ionization is specific to surface sites.[51] The argument is, under the current circumstance, that HCl may be

partially ionized. If we adapt this argument, in the classical adsorption treatment, we can approximately treat HCl as "molecularly" adsorbed on the surface. Equation 24 was based on this argument and should be considered as an empirical approach. In the pressure range $10^{-5}-10^{-7}$ Torr, eq 24 fits the experimental results well. We should point out that, if one examined the fittings in a limited pressure range, it is difficult to rule out a proposed mechanism.

The conclusion of this discussion is that the reaction follows the Langmuir−Hinshelwood mechanim at 190 K. HCl is in a dissociative form at 190 K. At the warmer temperature, the empirical kinetic model with a (partially) molecularly adsorbed HCl can fit the experimental observation. Previous study showed that the HOCl + HBr(s) → ClBr + $H_2O$(s) reaction followed the Eley−Rideal mechanism experimentally.[19] That was the difference in the mechanism between the two reactions.

**Effect of the Temperature on HOBr+ HCl → BrCl + $H_2O$.** The experimental observation of the lower reaction probability at the warmer temperature can be explained from eq 22 or 24. At the warmer temperature, the uptake coefficient of HOBr is lower (see Figure 8), so $b_{HOBr}$ is lower or $k_4$ (eq 19) is higher. More importantly, HCl desorbs from the ice film at 210−220 K. At 222 K, the HCl desorption rate is higher, i.e., $k_2 > k_1$, and $b_{HCl}P_{HCl}$ is decreased substantially. Thus, the overall reaction probability $\gamma$ in eq 22 or 24 is reduced qualitatively at 222 K.

**Comparison.** We may compare our study to previous measurements of HOBr uptake on ice. Abbatt[9] reported the uptake coefficient was 0.0017 at 228 K. Allanic et al.[16] reported that $\gamma$ was in the range 0.11−0.27 at 190 K and 0.05−0.15 at 200 K, which is shown in Figure 3. Results from this study are 0.11 at 190 K, 0.04 at 200 K, and 0.0012 at 230 K. Within the uncertainty of the measurement, this study is in excellent agreement with both published studies. This study showed that the lower $\gamma$ value at >220 K is due to HOBr desorption from the ice surface.

For the reaction of HOBr + HCl(s) → BrCl + $H_2O$(s), Allanic et al.[16] reported that the reaction probability was 0.25−0.42 at 190 K and 0.17−0.29 at 200 K with $P_{HOBr} = 10^{-6}-10^{-7}$ Torr. Two different HCl doping levels were used, which corresponded to a solid solution (quasi-liquid layer) and a liquid layer of HCl solutions above the solid ice. $P_{HCl}$ was on the order of $10^{-5}$ Torr according to our best estimate. We obtained that $\gamma_g = 0.24$ at 190 K and $\gamma_g = 0.16$ at 200 K at a slightly lower $P_{HCl}$. The $\gamma_g$ value is expected to be slightly lower than the one reported by Allanic et al. according to eq 22. The comparison is shown in Figure 7. Abbatt reported that $\gamma$ was 0.25 at 228 K and $P_{HOBr} < 2 \times 10^{-5}$ Torr and $P_{HCl} = 2.4 \times 10^{-5}$ Torr.[9] Under similar $P_{HCl}$ conditions, this study reported $\gamma_g = 0.19$ at 222 K (see Figure 6). Within the uncertainties of measurement, this study is in good agreement with both previous studies.

$\gamma_g$ of this reaction at 190 K is slightly lower than that of HOCl + HBr → ClBr + $H_2O$.[19] One possible explanation is that Br is a better nucleophile to donate its unshared electron pair with HOCl (see below), which results in a slightly faster rate. At the warmer temperature, the rate depends on the collision probability of the reactants. All reactants in these two reactions at 222 K are either desorbed or near $T_d$. $T_d$ of HOCl is about 170 K.[52] Qualitatively speaking, the collision probability of HOCl to adsorbed HBr decreases at a higher temperature.[19] The collision probability between two adsorbed species may not change substantially (assuming molecules are hopping across the surface), and the HOBr + HCl reaction showed a slightly higher rate than the HOCl + HBr reaction at 222 K. This is the case where the rate of the Langmuir−Hinshelwood type reaction is higher than that of the Eley−Rideal type.[53]

**CHART 1**

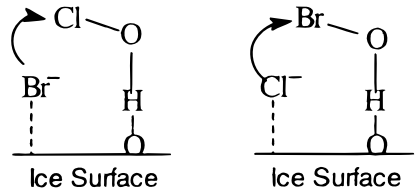


*Product BrCl*. Previous study showed that the product, BrCl, in the HOCl + HBr(s) → BrCl + $H_2O$(s) (rxn 1) reaction was nearly undetectable in the gas phase.[19] This and other studies indicated that the gas-phase product, BrCl, in the HOBr + HCl(s) → BrCl + $H_2O$(s) (rxn 2) reaction was observed (see Figure 2).[9,16] We propose the difference between two reactions is the nature of the HBr interaction with ice versus the HCl interaction with ice. In rxn 1, HBr adsorbs on the ice surface and may form hydrates under our experimental conditions ($P_{HBr} = 10^{-7}-10^{-6}$ Torr).[17,54] The hydrate is an ionic compound.[55] In rxn 2, HCl is dissociatively adsorbed on the ice surface at 190 K.[26,50,56] We assume that both rxn 1 and rxn 2 follow the nucleophilic reaction as analogous to the HOCl + HCl(s) → $Cl_2$ + $H_2O$(s) reaction. That is,

$$\mathrm{HOBr} + \mathrm{Cl}^- \rightarrow [\mathrm{HOBr}]\mathrm{Cl}^- \qquad (25)$$

for rxn 2 and

$$\mathrm{HOCl} + \mathrm{Br}^- \rightarrow [\mathrm{HOCl}]\mathrm{Br}^- \qquad (26)$$

for rxn 1. The critical issue is the structure of the intermediate. Quantum calculations suggest that the hydrogen end of the HOX molecule is bonded to the oxygen atom of $H_2O$.[57,58,33] The expected structures for the intermediates for rxns 1 and 2 are shown in Chart 1. Note that the intermediate of rxn 1 involves a ClBr···ice bond and rxn 2 has a BrCl···ice bond. The Br−ice interaction can be further modified by the formation of HBr hydrates near the ice surface in rxn 1. The desorption temperature of HBr (∼224 K[19]) from the ice film is about 5−10 K higher than that of HCl from the ice film. This indirectly suggests that the Cl···ice surface bond is weaker than the Br···ice surface bond. This qualitatively explained ClBr formed in rxn 2 might desorb back to the gas phase. BrCl intermediate in rxn 1 might be bounded to the surface because of the stronger interaction. In addition, BrCl intermediate in rxn 1 can react with adsorbed HBr to form $Br_2$.[59,19] A similar reaction was found in the solution as well.[60] This was the reason that BrCl was not observed in the HOCl + HBr reaction.

**Atmospheric Implications.** The study showed that the uptake coefficient of HOBr on the ice surface was about 0.1 at 190−200 K. The significance of this finding in atmospheric chemistry is that clouds and aerosols in the polar atmosphere can efficiently scavenge by HOBr molecules.

We may extrapolate the measured reaction probability for the HOBr + HCl(s) → BrCl + $H_2O$(s) reaction to $P_{HCl} \approx 10^{-7}$ Torr, the polar atmospheric conditions. $\gamma$ is approximately 0.05. Clearly, this reaction is not as efficient as $ClONO_2$ + HCl(s) → $Cl_2$ + $H_2O$(s) ($\gamma \approx 0.3$) to activate HCl on the PSC surfaces.[7] This reaction may affect the ozone distribution in several ways we will qualitatively discuss here. First, this reaction can activate HCl into BrCl on the ice surface or type-II PSC surfaces at 190 K. Second, HOBr is converted to BrCl

in the low sunlight or dark condition. The lifetime of BrCl is about 60 s and HOBr is about 1000 s in the midlatitude of the lower stratosphere.[11] The reaction may not activate Br, but it can change the partitioning of HOBr to BrCl and the photolysis of HOBr; thus, it decreases the OH and $HO_2$ concentration and subsequently impacts the HCl/Cl concentration. Finally, the important contribution of this reaction is to change the partitioning of bromine and chlorine in the lower stratosphere. Lary et al. proposed this is important heterogeneous bromine on PSCs to consider.[14] The atmospheric chemistry modeling calculations are required to fully assess the impact of ozone depletion.

This reaction becomes less efficient to activate HCl and HOBr at the warmer tropospheric temperature (220−240 K). The typical heterogeneous gas collision time $\tau_c$ is on the order of 20 s in the troposphere. A heterogeneous reaction with a lower $\gamma = 10^{-3}-10^{-4}$ is still considered to be a significant process in the troposphere.[61] This reaction could potentially activate chlorine on the cirrus clouds and tropospheric snow surfaces.

**Summary.** Some main conclusions can be summered as follows: the uptake coefficient of HOBr on ice surfaces was determined at 190−239 K as shown in Figure 3. HOBr molecules desorbed from the ice surface under the flow-tube condition were reported in the range of 214−229 K. The nature of uptake coefficient was explored in terms of the fundamental gas−surface interaction. The reaction probability $\gamma_g$ for the HOBr + HCl(s) → BrCl + $H_2O$(s) reaction ranges from 0.05 to 0.23 at 190 K and 0.004 to 0.19 at 222 K. Kinetic analysis suggested that the heterogeneous reaction follows the Langmuir−Hinshelwood type. This reaction may play a role in the activation of HCl and change the bromine and chlorine partitioning in the lower stratosphere and troposphere.

**Acknowledgment.** The authors thank Professors John C. Tully and Steven L. Bernasek for helpful discussion and two anonymous reviewers for helpful suggestions and comments on the manuscript. This work was supported by the National Science Foundation under Grant ATM-9530659.

## References and Notes

(1) Solomon, S.; Garcia. R. R.; Rowland, F. S.; Wuebbles, D. J. *Nature* **1986**, *321*, 755.

(2) *Scientific Assessment of Ozone Depletion: 1994*; Report 37; World Meteorolgical Organization: Geneva, 1995; Chapters 3 and 10.

(3) Solomon, S. *Nature* **1990**, *347*, 347.

(4) Molina, M. J.; Molina, L. T.; Kolb, C. E. *Annu. Rev. Phys. Chem.* **1996**, *47*, 327.

(5) Rossi, M. J. *Chimia* **1996**, *50*, 199.

(6) Brune, W. H. In *Perspectives in Environmental Chemistry*; Macalady, D. L., Ed.; Oxford: New York, 1998; Chapter 6.

(7) DeMore, W. B.; Sander, S. P.; Golden, D. M.; Hampson, R. F.; Kurylo, M. J.; Howard, C. J.; Ravishankara, A. R.; Kolb, C. E.; Molina, M. J. *Chemical Kinetics and Photochemical Data for Use in Stratospheric Modeling*; Evaluation no. 12; JPL: Pasadena, 1997; pp 230−244.

(8) Hanson, D. R.; Ravishankara, A. R. *Geophys. Res. Lett*. **1995**, *22*, 345.

(9) Abbatt, J. P. D. *Geophys. Res. Lett*. **1994**, *21*, 665.

(10) Abbatt, J. P. D. *J. Geophys. Res*. **1995**, *100*, 14009.

(11) Lary, D. J. *J. Geophys. Res.* **1996**, *101*, 1505.

(12) Polet, G.; Pirre, M.; Maguin, F.; Ramaroson, R.; Le Bras, G. *Geophys. Res. Lett.* **1992**, *19*, 2305.

(13) Hanson, D. R.; Ravishankara, A. R. In *The Tropospheric Chemistry of Ozone in the Polar Regions*; Niki, H., Becker, K. H., Eds.; NATO ASI Series; Springer-Verlag: New York, 1993; pp 281−290.

(14) Lary, D. J.; Chipperfield, M. P.; Toumi, R.; Lenton, T. *J. Geophys. Res.* **1996**, *101*, 1489.

(15) Solomon, S.; Garcia, R. R.; Ravishankara, A. R. *J. Geophys. Res*. **1994**, *99*, 20491.

(16) Allanic, A.; Oppliger, R.; Rossi, M. J. *J. Geophys. Res.* **1997**, *102*, 23529.

(17) Chu, L. T.; Heron, J. W. *Geophys. Res. Lett*. **1995**, *22*, 3211.

(18) Chu, L. T. *J. Vac. Sci. Technol. A* **1997**, *15*, 201.

(19) Chu, L.; Chu, L. T. *J. Phys. Chem.* A **1999**, *103*, 691.

(20) Keyser, L. F.; Leu, M.-T.;*J. Colloid Interface Sci.* **1993**, *155*, 137.

(21) Haynes, D. R.; Tro, N. J.; George, S. M. *J. Phys. Chem*. **1992**, *96*, 8502.

(22) Chapin, R. M. *J. Am. Chem. Soc.* **1934**, *56*, 2211.

(23) Brown, R. L. *J. Phys. Natl. Bur. Stand. (U.S.)* **1978**, *83*, 1.

(24) Keyser, L. F.; Moore, S. B.; Leu, M.-T. *J. Phys. Chem.* **1991**, *95*, 5496.

(25) Keyser, L. F.; Leu, M.-T.; Moore, S. B. *J. Phys. Chem.* **1993**, *97*, 2800.

(26) Chu, L. T.; Leu, M.-T.; Keyser, L. F. *J. Phys. Chem.* **1993**, *97*, 7779.

(27) Chu, L. T.; Leu, M.-T.; Keyser, L. F. *J. Phys. Chem*. **1993**, *97*, 12798.

(28) Keyser, L. F.; Leu, M.-T. *Microscopy Res. Technique* **1993**, *25*, 343.

(29) $N_L = ax^b + N \log(x + c)$ where $a = -0.1037$, $b = 4.6841 \times 10^{-15}$, $N = 10.6290$, and $c = 0.8690$. $x$ (=0.5−35) is the film thickness in micrometers. The parameters were derived from references 25 and 26. This expression is valid for a thin ice film at about 200 K.

(30) Tully, J. C. *Annu. Rev. Phys. Chem*. **1980**, *31*, 319.

(31) Gerber, R. *Chem. Rev*. **1987**, *87*, 29.

(32) Kroes, G.-J.; Clary, D. C. *J. Phys. Chem*. **1992**, *96*, 7079.

(33) Ying, L.; Zhao, X. *J. Phys. Chem. A* **1997**, *101*, 3569.

(34) Masel, R. I. *Principles of Adsorption and Reaction on Solid Surfaces*; Wiley: New York, 1996; Chapters 3 and 7.

(35) Rudzinski, R.; Everett, D. H. *Adsorption of Gases on Heterogeneous Surfaces*; Academic Press: New York, 1992; Chapter 1.

(36) Binder, K.; Landau, D. P. *Surf. Sci*. **1981**, *108*, 503.

(37) Binder, K.; Landau, D. P. In *Advances in Chemical Physics*; Lawley, K. P., Ed.; Wiley: New York, 1989; p 91.

(38) Chu, L. T.; Chu, L. *J. Phys. Chem.* B **1997**, *101*, 6271.

(39) Pauling, L. *The Nature of the Chemical Bond*, 3rd ed.; Cornell University Press: Ithaca, 1960; pp 257−264.

(40) Boudart, M.; Djega-Mariadassou, G. *Kinetics of Heterogeneous Catalytic Reactions*; Princeton University Press: Princeton, 1984; Chapter 2.

(41) Atkins, P. W. *Physical Chemistry*, 2nd ed.; Freeman: San Francisco, 1982; pp 1016−1021.

(42) Berland, B. S.; Tolbert, M. A.; George, S. M. *J. Phys. Chem. A* **1997**, *101*, 9954.

(43) Davy, J. G.; Somorjai, G. A. *J. Chem. Phys*. **1971**, *55*, 3624.

(44) George, S. M. Livingston, F. E. *Surf. Rev. Lett.* **1997**, *4*, 771.

(45) Livingston, F. E.; George, S. M. *J. Phys. Chem. A* **1998**, *102*, 10280.

(46) Assume the diffusion coefficient of HOBr in ice to be $D = 10^{-10}-10^{-12}$ $cm^2/s$ at 220 K. The diffusion length $z$ is about a micrometer and it is about the thickness of $10^3$ ice bilayers (BL).

(47) Flückiger, B.; Thielmann, A.; Gutzeiller, L.; Rossi, M. J. *Ber. Bunsen-Ges. Phys. Chem*. **1998**, *102*, 915.

(48) Given $T_d = 210$ K, the activation energy of the desorption $E_a$ is estimated to be 12 kcal/mol (see p 513 of ref 34). Residence time $\approx 1/(k_o \exp(-E_a/kT))$.

(49) Robertson, S. H.; Clary, D. C. *Faraday Discuss*. **1995**, *100*, 309. Adsorption mean time $\tau_p \approx 10^{-7}$ s.

(50) Gertner, B. J.; Hynes, J. T. *Science* **1996**, *271*, 1563.

(51) Bianco, R.; Gertner, B. J.; Hynes, J. T. *Ber. Bunsen-Ges. Phys. Chem*. **1998**, *102*, 518.

(52) Horn, A. B.; Sodeau, J. R.; Roddis, T. B.; Williams, N. A. *J. Phys. Chem. A* **1998**, *102*, 6107.

(53) Weinberg, W. H. In *Dynamics of Gas−Surface Interactions*; Rettner, C. T., Ashfold, M. N. R., Eds.; The Royal Society of Chemistry: Cambridge, 1991; Chapter 5.

(54) Chu, L. T.; Chu, L. *J. Phys. Chem. A* **1999**, *103*, 384.

(55) Lundgren, J.-O. *Acta Cryst*. **1970**, *B26*, 1893.

(56) Bahnam, S. F.; Horn, A. B.; Koch, T. G.; Sodeau, J. R. *Faraday Discuss*. **1995**, *100*, 321.

(57) Brown, A. R.; Doren, D. J. *J. Phys. Chem. B* **1997**, *101*, 6308.

(58) Dibble, T. S.; Francisco, J. S. *J. Phys. Chem*. **1995**, *99*, 1919.

(59) Hanson, D. R.; Ravishankara, A. R. *J. Phys. Chem*. **1992**, *96*, 9441.

(60) Wang, T. X.; Kelley, M. D.; Cooper, J. N.; Beckwith, R. C.; Margerum, D. W. *Inorg. Chem*. **1994**, *33*, 5872.

(61) Kolb, C. E.; Worsnop, D. R.; Zahniser, M. S.; Davidovits, P.; Keyser, L. F.; Leu, M. T.; Molina, M. J.; Hanson, D. R.; Ravishankara, A. R.; Williams, L. R.; Tolbert, M. A. In *Progress and Problems in Atmospheric Chemistry*; Baker, J. R., Ed.; World Scientific: Singapore, 1995; pp798−804.